Neurobiology of Disease 135 (2020) 104704

Contents lists available at ScienceDirect

Neurobiology of Disease

journal homepage: www.elsevier.com/locate/ynbdi

Implications of gut microbiota dysbiosis and metabolic changes in prion disease

Dongming Yang[a], Deming Zhao[a], Syed Zahid Ali Shah[b], Wei Wu[a], Mengyu Lai[a], Xixi Zhang[a], Jie Li[a], Zhiling Guan[a], Huafen Zhao[a], Wen Li[a], Hongli Gao[a], Xiangmei Zhou[a], Lifeng Yang[a,*]

[a] Key Laboratory of Animal Epidemiology and Zoonosis, Ministry of Agriculture, National Animal Transmissible Spongiform Encephalopathy Laboratory, College of Veterinary Medicine, China Agricultural University, Beijing, China
[b] Department of Pathology, Faculty of Veterinary Sciences, Cholistan University of Veterinary and Animal sciences, Bahawalpur, Pakistan

ARTICLE INFO

Keywords:
Prion infection
Microbiome
Metabolomics
Short chain fatty acids
Multi-omics analysis

ABSTRACT

Evidence of the gut microbiota influencing neurodegenerative diseases has been reported for several neural diseases. However, there is little insight regarding the relationship between the gut microbiota and prion disease. Here, using fecal samples of 12 prion-infected mice and 25 healthy controls, we analyzed the structure of the gut microbiota and metabolic changes by 16S rRNA sequencing and LC-MS–based metabolomics respectively as multi-omic analyses. Additionally, SCFAs and common amino acids were detected by GC–MS and UPLC respectively. Enteric changes induced by prion disease affected both structure and abundances of the gut microbiota. The gut microbiota of infected mice displayed greater numbers of *Proteobacteria* and less *Saccharibacteria* at the phylum level and more *Lactobacillaceae* and *Helicobacteraceae* and less *Prevotellaceae* and *Ruminococcaceae* at the family level. A total of 145 fecal metabolites were found to be significantly different in prion infection, and most (114) of these were lipid metabolites. Using KEGG pathway enrichment analysis, we found that 3 phosphatidylcholine (PC) compounds significantly decreased and 4 hydrophobic bile acids significantly increased. Decreases of 8 types of short-chain acids (SCFAs) and increases of Cys and Tyr and decreases of His, Trp, and Arg were observed in prion infection. Correlation analysis indicated that the gut microbiota changes observed in our study may have been the shared outcome of prion disease. These findings suggest that prion disease can cause significant shifts in the gut microbiota. Certain bacterial taxa can then respond to the resulting change to the enteric environment by causing dramatic shifts in metabolite levels. Our data highlight the health impact of the gut microbiota and related metabolites in prion disease.

1. Introduction

Prion disease, or transmissible spongiform encephalopathies, are a class of fatal neurodegenerative diseases that can affect both humans and some domesticated and free-ranging animal species. There are currently no treatments for prion disease, resulting in high societal and economic costs (Bruce et al., 1997). Prion disease are commonly characterized by the presence of aggregates of the relatively proteinase-resistant isoform (PrP^{Sc}) of the host cellular protein PrP^{c}, primarily in neural tissue (Legname et al., 2004; Manson et al., 1994). The accumulation of PrP^{Sc} in the central nervous system affects a diverse range of cellular and physiological functions, such as cognition, signal transduction, and seizure sensitivity and is associated with extensive neuropathologies, such as the activation of microglia (Prinz and Priller, 2014), inflammation, and phagocytosis of apoptotic cells (De Almeida et al. De Almeida et al., 2005). Many prion disease are acquired by oral

Abbreviations: AD, Alzheimer's disease; ANOVA, The analysis of variance; AUC, area under receiver operating characteristic curve; BSTFA, *N,O*-Bis(trimethylsilyl) trifluoroacetamide; COG, clusters of orthologous group; DE, anhydrous diethylether; EI, electron impact; FC, fold-change; GC-MS, gas chromatography–mass spectrometry; GMBA, gut-microbiota-brain axis; KEGG, Kyoto Encyclopedia of Genes and Genomes; LC-MS, liquid chromatography-mass spectrometry; LDA, linear discriminant analysis; LEfSe, Linear discriminant analysis effect size; MVA, Multivariate analysis; NMDS, non-metric multi-dimensional scaling; OPLS-DA, orthogonal projections to latent structures discriminant analysis; OTUs, Operational taxonomic units; PC, phosphatidylcholine; PCoA, principal component analysis; PCoA, principal coordinates analysis; PD, Parkinson's disease; PE, phosphatidylethanolamine; PI, phosphatidylethanolamine; PICRUSt, Phylogenetic Investigation of Communities by Reconstruction of Unobserved States; PS, phosphatidylserine; QIIME, Quantitative Insights Into Microbial Ecology; RDA, Redundancy analysis; RF, Random; SCFAs, short-chain acids; UPLC, Ultra-performance liquid chromatography; VIP, The variable importance in projection

* Corresponding author.
E-mail address: yanglf@cau.edu.cn (L. Yang).

https://doi.org/10.1016/j.nbd.2019.104704
Received 6 August 2019; Received in revised form 22 November 2019; Accepted 8 December 2019
Available online 16 December 2019

consumption of contaminated food or pasture. PrP^{Sc} initially appears in intestinal neurons and gut-associated lymphoid tissues within the intestinal lining, including the tonsils, Peyer's patches, appendix, and colonic and cecal patches, together with the mesenteric lymph nodes (Hilton et al., 1998; Mabbott et al., 2003). The early replication of prions in the intestines has been found to be essential for its spread to the brain (Laura et al., 2011; Montrasio et al., 2000) and the intestinal luminal epithelium is also involved in transportation of PrP^{Sc} (Donaldson et al., 2016; Heppner et al., 2001; Marshall et al., 2018), which suggests that the pathogenic agent may cause disorder in the gut environment and thus result in a series of complex alterations to cellular metabolism, which may further intensify prion infection in the brain.

The gut microbiota, regarded as “the forgotten organ”, is home to 100 trillion bacteria, as well as some fungi, archaea, and viruses, and is comprised of 10-fold more cells than the human body. Research efforts have gradually uncovered that the gut microbiota plays a key role in the normal function of the brain and nervous system via many mechanisms. These connections act as a bidirectional communication pathway between the gut microbiota and neural systems involved in many neurological diseases, such as Parkinson's disease (PD), Alzheimer's disease (AD) (Abbott et al., 2001; Girolamo et al., 2017; Lei et al., 2016; Pryde et al., 2002; Rhee et al., 2009). However, no related studies to date have addressed whether prion disease may influence the gut microbiota.

The gastrointestinal tract provides relatively stable living conditions for the gut microbiota, which performs nutritional, protective, and metabolic functions for its host. A stable gastrointestinal tract environment is vital for balance of gut microbes and maintaining the health of hosts. Although there is no gold standard to assess this “healthy” gut microbiota, changes in the composition and diversity of the gut microbial community may influence metabolic functions of the host and increase risk for poor health outcomes. We hypothesize that the altered intestinal environment caused by prion disease may alter the gut microbiota and thereby affect the metabolism of the host, which may in turn intensify the prion disease. The gut microbiota may be another mechanism by which prion pathogens exert their effect. Identification of the microbiota-driven mechanisms underlying the link between metabolic shifts and prion disease holds extraordinary promise for developing microbiota-driven intervention strategies as treatments for prion disease.

In this study, we analyzed and compared the microbiota composition and metabolites in fecal samples from mice with prion disease and those of their healthy littermates using 16S rRNA gene sequencing and metabolomics. The association of the gut microbiota with differential metabolite levels induced by prion disease was further examined to explore the relationship between the gut microbiota, associated metabolic pathways, and prion disease. This study is the first to reveal the health impacts of prion disease from the perspective of the gut microbiota and related metabolism.

2. Materials and methods

2.1. Study design and sample collection

Thirty-seven six-week-old C57Bl/6 female mice purchased from Beijing Vital River Laboratory Animal Technology Co., Ltd. were housed in standard cages in a specific pathogen-free facility with a 12:12-h light:dark photoperiod. The mice were randomly divided into 2 groups (25 for the infected group, 12 for the control group), and were housed in single cage. The mice were injected each with 10 μL 10% brain homogenate (scrapie RML strain, infected group) or 10 μL deionized water (control group) into their cerebral ventricle. After 150 days, we immediately collected fresh fecal pellets from the colonic tissue of each mouse (all animals were in the agonal stage) using sterile sampling containers. Fecal pellets were immediately frozen in liquid nitrogen and transferred to the laboratory. Each sample was subpacked into two 1.5-mL Eppendorf tubes and stored at −80 °C until DNA and metabolite extraction (performed in an aseptic operation box). Animal experiments were approved and performed in accordance with the guidelines of the Institutional Animal Care and Use Committee of China Agricultural University.

2.2. DNA extraction and Illumina MiSeq sequencing

DNA from samples was extracted using the EZNA Soil DNA Kit (Omega Bio-tek, Norcross, GA, USA) according to manufacturer's instructions. The V3-V4 region of the bacterial 16S rRNA gene was amplified by PCR (primers: 341F, 5′-barcode-CCTACGGGNBGCASCAG-3′ and 805R, 5’-GACTACNVGGGTATCTAATCC-3′), where “barcode” is an eight-base sequence unique to each sample. PCR amplification and sequencing of the PCR amplicons are summarized in the Supplementary Methods. Purified amplicons were pooled in equimolar amounts and paired-end sequenced (2 × 250) on the Illumina MiSeq platform according to the standard protocols. The raw reads were deposited into the NCBI Sequence Read Archive (SRA) database (accession number: SRP186619).

2.3. LC-MS–based metabolism analysis

Approximately 40 mg of fecal sample was used for metabolite extraction. The fecal sample was extracted with 300 μL methanol-acetonitrile (2:1, *v*/v), and 20 μL L-2-chlorophenylalanine (0.3 mg/mL) was then added as the internal standard. After homogenizatoin and ultrasonic extraction, the samples were incubated at −20 °C for 30 min and centrifuged for 10 min at 10,000 rpm at 4 °C. Finally, 20 μL of supernatant from each sample was transferred to a vial for liquid chromatography-mass spectrometry (LC-MS) analysis. LC-MS analysis was performed on an Ultimate 3000-Velos Pro system equipped with a binary solvent delivery manager and a sample manager, coupled with a LTQ Orbitrap Mass Spectrometer equipped with an electrospray interface (Thermo Fisher Scientific, USA) using an Acquity BEH C18 column (100 mm × 2.1 mm i.d., 1.7 μM; Waters, Milford, USA). Chromatographic conditions are summarized in the Supplementary Methods.

2.4. Detection of SCFAs and amino acids

GC–MS (Gas chromatography–mass spectrometry) and UPLC (Ultra high performance liquid chromatography) were performed to analyze SCFAs and amino acids, respectively. To extract SFCAs, 100 mg fecal samples were combined, mixed with 500 mL sterile 18-Ω deionized water, homogenized by mixing three times at 6500 rpm for 20 s (Bertin Technologies, Montigmy le Bretonnexux, France), and centrifuged for 15 min at 13,000 rpm at 4 °C. Supernatants were mixed with 10 μL of 5 M analytical-grade hydrochloric acid to bring the pH to 2, and then 100 μL of anhydrous diethylether (DE) (1:1, *v*/v) was added. After centrifuging for 5 min at 10,000 rpm, the DE layer was transferred with anhydrous Na_2SO_4 to a new microtube. Then, 100 μL of DE extract was transferred into a glass insert in a GC vial. 5 μL of *N*,*O*-Bis(trimethylsilyl)trifluoroacetamide (BSTFA) was added and the mixture was capped tightly and vortexed for 5 s. The mixture was kept in the GC vial and incubated at 70 °C for 20–40 min and then at 37 °C for 2 h. GC–MS analysis was performed using an Agilent 7890A gas chromatography system coupled to an Agilent 5975C inert XL EI/CI mass spectrometric detector (MSD, Agilent Technologies, Santa Clara, CA). Derivatives were separated using an HP-5 ms capillary column coated with 5% phenyl 95% methylpolysiloxane (30 m × 250 i.d., 0.25 μm film thickness, Agilent J & W Scientific, Folsom, CA). One microliter of the derivatives was injected in split mode with a ratio of 10:1, and the solvent delay time was set to 2.2 min. The initial oven temperature was held at 50 °C for 2 min, ramped to 70 °C at a rate of 10 °C/min, to 85 °C at a rate of 3 °C/min, to 110 °C at a rate of 5 °C/min, to 290 °C at a rate

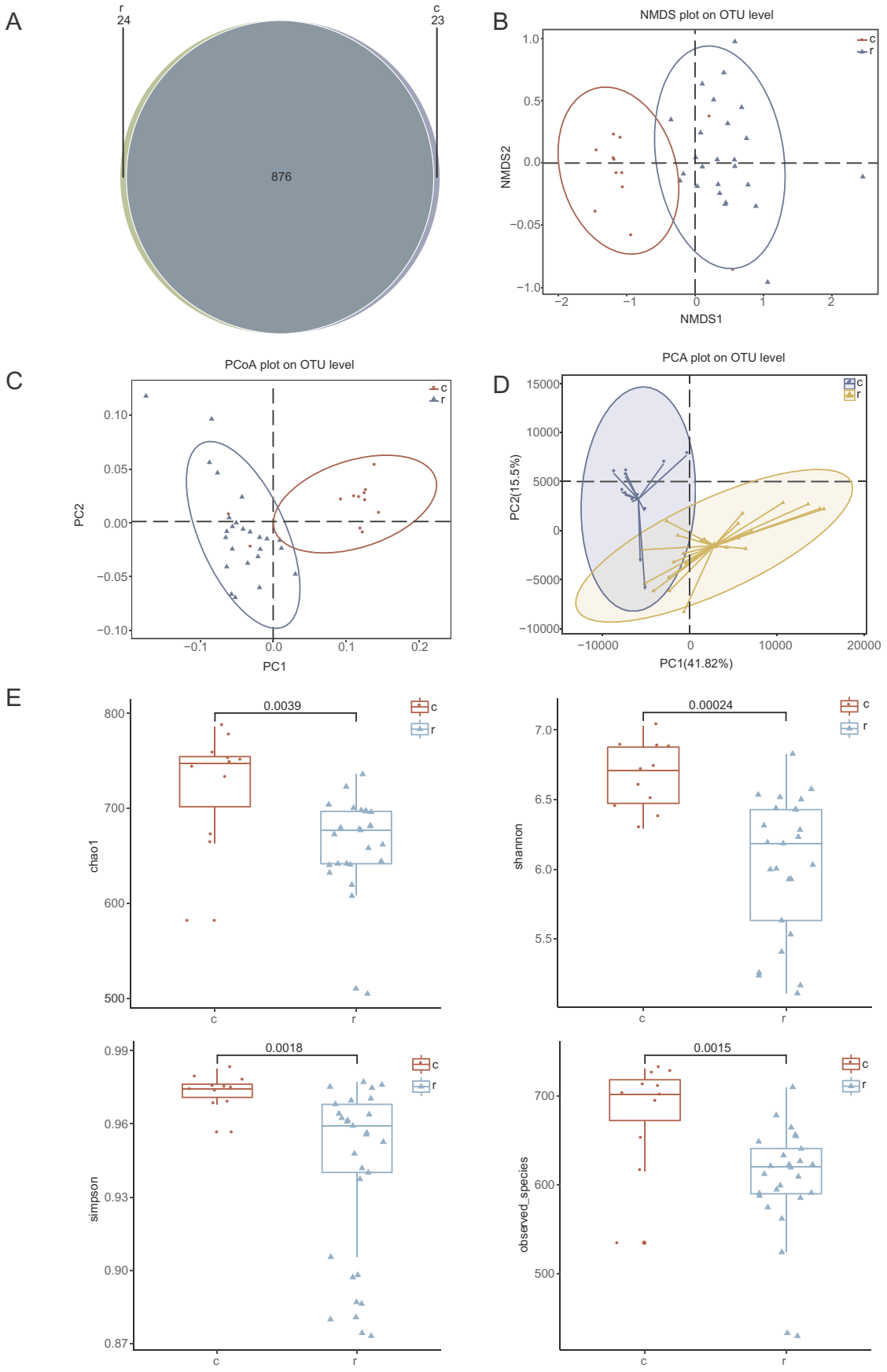

Fig. 1. Comparison of gut microbial structure between prion infectious groups and healthy controls. (A): The Venn diagram reflecting the overlap of OTUs in fecal microbiota in two groups. (B-D): Beta diversity metrics (plots of NMDS, PCoA, and PCA of unweighted UniFrac). (E): Alpha diversity metrics (the box plots of Chao1, the Shannon and Simpson, and observed species diversity indices), *p* value is displayed on the picture. Pairewise comparions using the wilcoxon rank sum test Abbreviations: R: fecal samples from prion infected mice. C: fecal samples from healthy control mice.

of 30 °C/min, and finally held at 290 °C for 8 min. Helium was used as a carrier gas at a constant flow rate of 1 mL/min through the column. The temperatures of the front inlet, transfer line, and electron impact (EI) ion source were set at 260 °C, 290 °C, and 230 °C, respectively. The electron energy was −70 eV, and the mass spectral data was collected in full scan mode (*m/z* 30–600).

To analyze amino acids, 40 mg of each fecal pellet was mixed with 100 μL of deionized water. The mixtures with internal standard solution (80 ng/mL) and methanol were vortexed for 1 min, incubated for 20 min on ice, and centrifuged for 15 min at 12,000 rpm at 4 °C. Supernatants were evaporated completely under a gentle stream of nitrogen at 40 °C and subjected to a derivatization procedure for D-amino acids. The residue was reconstituted with 50 μL acetonitrile-8 mM ammonium hydrogen carbonate (7:93, *v*/v), followed by 15 μL of 0.2 M sodium tetraborate and 200 μL of (*S*)-NIFE (1 mg/mL) diluted with acetonitrile by mixing for 1 min, followed by incubating with (*S*)-N-(4-nitrophenoxycarbonyl) phenylalanine methoxyethyl ester for 20 min at room temperature. Ten μL of 4 M hydrogen chloride and 125 μL of acetonitrile-8 mM ammonium hydrogen carbonate (7:93, *v*/v) were added and centrifuged at 12,000 rpm for 5 min at 4 °C to terminate the reaction. Two μL of the supernatant was injected for analysis. UPLC was performed on an Acquity system (Waters) equipped with a 2996 photodiode array detection (DAD) system. The column used was an ACCQ-TAGTMULTRA C18 column (100 mm × 2.1 mm i.d., 1.7 μM) from Waters. The flow rate was 0.7 mL/min, and the column temperature was kept at 50 °C. The injection volume was 1 μL, and the detection wavelength was set at 260 nm. The solvent system consisted of two eluents: (A) AccQ·Tagultra eluent A concentrate (5%, *v*/v) and water (95%, v/v); (B) AccQ·Tagultra eluent B. The following gradient elution was used: 0–0.54 min, 99.9% A-0.1% B; 5.74 min, 90.9% A-9.1% B; 7.74 min, 78.8% A-21.2% B; 8.04 min, 40.4% A-59.6% B; 8.70–10 min, 99.9% A-0.1% B.

2.5. Bioinformatics and statistical analysis

To analyze the bacterial community structure, raw fastq files were quality-filtered using Trimmomatic and merged using FLASH (criteria are summarized in the Supplementary Methods).The taxonomy of each 16S rRNA gene sequence was analyzed by the RDP Classifier algorithm (http://rdp.cme.msu.edu/) against the Silva (SSU123) 16S rRNA database with a confidence threshold of 70%. Many statistical analyses were conducted to calculate the differences between the infected and control groups. Specific parameters for alpha and beta diversities, linear discriminant analysis effect size (LEfSe) analysis, random forest (RF) models, and others are outlined in the Supplementary Methods. KEGG (Kyoto Encyclopedia of Genes and Genomes) pathways and clusters of orthologous group (COG) functions analysis was performed by the Phylogenetic Investigation of Communities by Reconstruction of Unobserved States (PICRUSt) methods based on 16S rRNA sequencing data and a database of reference genomes (Langille et al., 2013). Statistical differences (p value < 0.01) were further achieved using Welch's *t*-test in STAMP software.

For analysis of the perturbations and differences in metabolite levels, the metabolism data were mined using Progenesis QI (Waters Corporation, Milford, USA) and were then normalized and divided into a two-dimensional data matrix. Finally, 7071 features in the (ESI+) ion mode and 6757 features in the (ESI-) ion mode were achieved in this study. Specific details of the statistical analyses are summarized in the Supplementary Methods.

Data from the SCFA analysis were analyzed using MassHunter programs (version B.07.01, Agilent, USA). UItiMate 3000 UHPLC software (Thermo Fisher, USA) was used for system control and data acquisition. The SCFA and amino acid contents were calculated with external standard methods.

3. Results

3.1. Deep sequencing of the 16S rRNA gene

There is evidence connecting neurodegenerative diseases with gut microbiota disorder. Thus, the gut microbiota may also play an essential role in the processes underlying those diseases. To assess gut microbiota changes in prion disease, we used 16S rRNA sequencing to analyze 37 fecal samples. Sequencing on the Illumina MiSeq platform generated a total of 5,640,408 raw reads (an average of 173,321.4 and 142,422 reads for the control and infected groups, respectively). We obtained 4,941,236 clean reads after contig assembly and filtering (mean reads of 150,169.3 and 125,568.2 for the control and infected groups, respectively). We identified 923 total operational taxonomic units (OTUs) at a 97% similarity level. Of these, 876 were shared between the two groups, and 24 and 23 OTUs were specific to the control and infected groups, respectively (Fig. 1A).

3.2. Gut microbiota responses to enteric changes in prion infection

Alpha diversity metrics (Chao1, the Shannon and Simpson and observed species diversity indices) were calculated, and significant statistical differences between the gut microbiota of the infected and control groups were assessed using generalized linear models implemented in the R platform. All four indices, including Chao1, the Shannon and Simpson and observed species indices were higher for the control group than for the infected group. The *p*-values of those four metrics were all < 0.05 (Fig. 1E) indicating that the infected group displayed significantly less diversity and richness in their gut microbiota. For beta diversity, we used NMDS, PCoA, and PCA ordination of unweighted UniFrac distances (Fig. 1B–D) to display the discrepancy between the groups. We found that the gut microbiota composition of the infected group was distinct from that of the control group (ANOSIM, $r = 0.15$, $p = 0.030$). PCoA and PCA (PC1 = 41.82%, PC2 = 15.5%) revealed a pronounced separation of the infected and control groups and little distance in the diversity of samples from the same group, indicating a significant difference between the groups.

To identify the types of bacterial taxa that varied between groups, we employed LEfSe analysis, an algorithm for high-dimensional biomarker discovery, which uses LDA to estimate the effect size of each taxon differentially represented in the infected and control groups. LEfSe (Fig. 2B) identified 20 discriminative features (LDA ≥ 3) whose relative abundances varied significantly between the infected and control groups. At the phylum level, *Proteobacteria* were enriched in the infected group, while *Saccharibacteria* displayed the opposite trend. At the family level, two microbiota members, *Lactobacillaceae* and *Helicobacteraceae*, were increased in the infected group, and three microbiota members (*UnknownFamily*, *Ruminococcaceae,* and *Prevotellaceae*) were decreased in the infected group. Among these four microbiota members, at the family level, the *Lactobacillaceae* and *Prevotellaceae* displayed the most dramatic increase and decrease, respectively. A cladogram (Fig. 2A) shows the structure of the fecal microbiota and the predominant bacteria among the prion-infected and control groups, revealing that the greatest shifts in the composition of the microbiota were primarily in *Proteobacteria* and *Saccharibacteria*.

To evaluate prion infection status based on an ensemble of decision trees, we used the RF method to build a predictive model based on the fecal microbial samples. We used the taxa that displayed significantly different abundances with the result of LEfSe analysis in the Wilcoxon rank-sum test as the input. Using the RF model (Fig. 2C), we predicted 17 genera from the fecal samples. A mean classification error of 0.17 was achieved, and the area under the receiver operating characteristic curve (AUC) was 0.9. Together, these data indicate that the gut microbiota exhibits several significant changes both in structure and diversity that are associated with prion disease.

To determine changes of potential functions of the intestinal

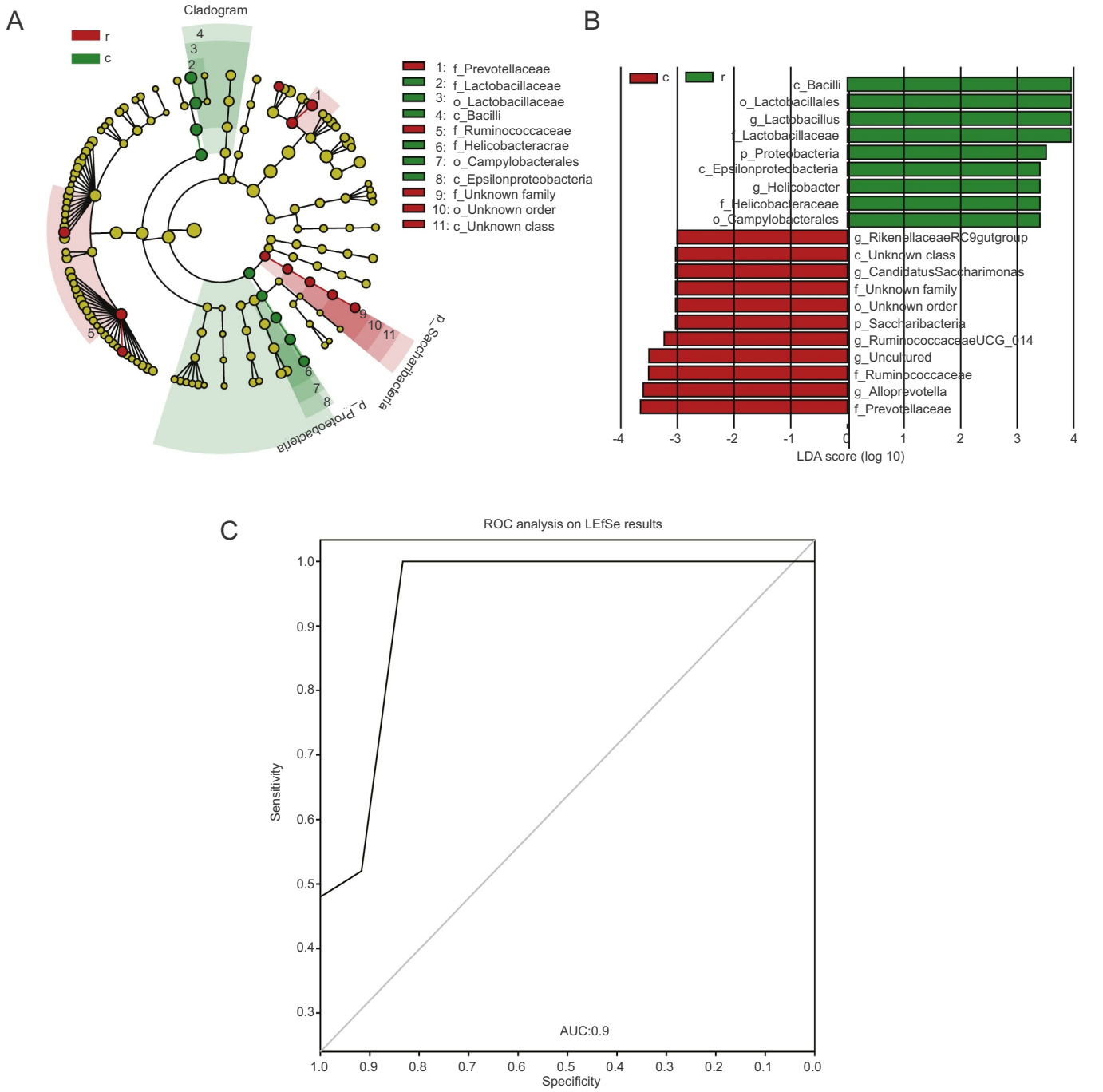

Fig. 2. Differentially abundant bacterial taxa between prion infectious groups and healthy control groups. (A): LDA scores for the differential abundance of bacterial taxa. Bacterial taxa significantly enriched in the R groups (LDA score ≥ 3) or C groups (LDA score ≤ −3) were made by LEfSe analysis. (B): Cladogram made by LEfSe reflecting differentially abundance of bacterial taxa. (C): ROC curve made by the RF using changed bacterial taxa of fecal microbiota. The AUC (area under the ROC curve) is 0.9 representing the corresponding optimal threshold. Abbreviations: R: fecal samples from prion infected mice. C: fecal samples from healthy control mice. (p < 0 .05). (D_1: Phylum, D_2: Class, D_3: Order, D_4: Family, D_5: Genus).

bacterial communities that may be altered in prion disease, we use PICRUSt analysis to predict COG functions and KEGG pathways. A total of 25 COG terms and 206 KEGG pathways were generated by the prediction. Using Welch's *t*-test to compare the altered pathways, we found only Chromatin structure and dynamics was significantly increased (p value < 0.01) in prion disease, as Carbohydrate transport and metabolism, Cell wall/membrane/envelopebiogenesis, General function prediction, and Amino acid transport and metabolism were the most abundant pathways (Fig. 3A). Furthermore, 24 KEGG pathways were selected showing significantly altered in prion disease (p value < 0.01). Among those, Primary immunodeficiency, Apoptosis, Taurine and hypotaurine metabolism, and Nucleotide metabolism were the maximum increase in prion disease, which were concerned in the microbial chromatin structure and dynamics function, while Fatty acid metabolism, Basal transcription factors, Caprolactam degradation, Carotenoid biosynthesis, and Meiosis-yeast showed significant decreased in prion disease(Fig. 3B).

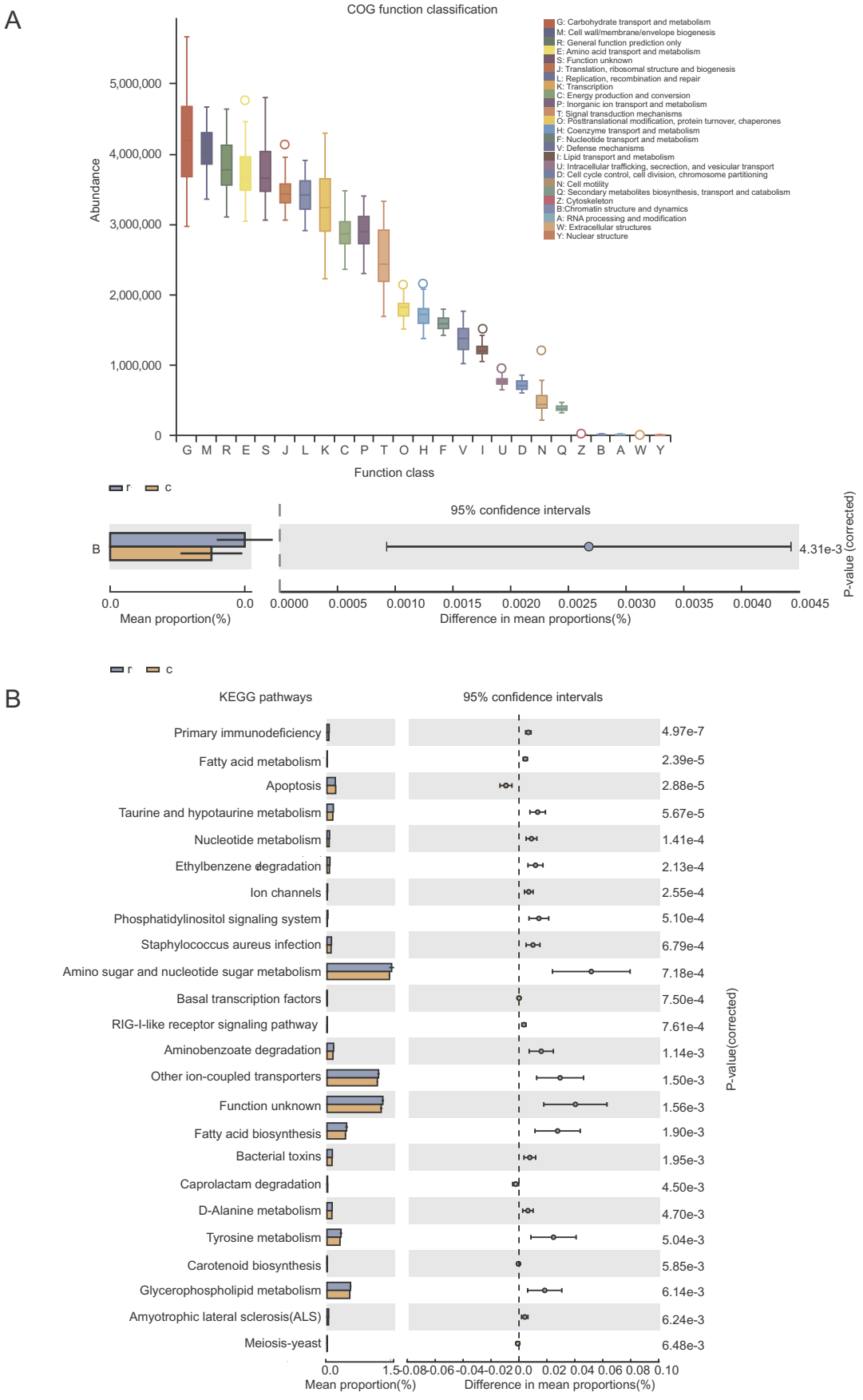

Fig. 3. Box and extended error bar plots indicating the functional differences of fecal microbiota in prion infectious groups and healthy control groups. (A): COG and (B): KEGG categories were obtained from 16S rRNA gene sequence using PICRUSt. Significant differences between two groups were tested using Welch's *t*-test (p value < 0.05). The KEGG pathways with the difference in mean proportion effect size $> 0.0005\%$ or 0.02% were separated by dotted lines. Abbreviations: R: fecal samples from prion infected mice. C: fecal samples from healthy control mice.

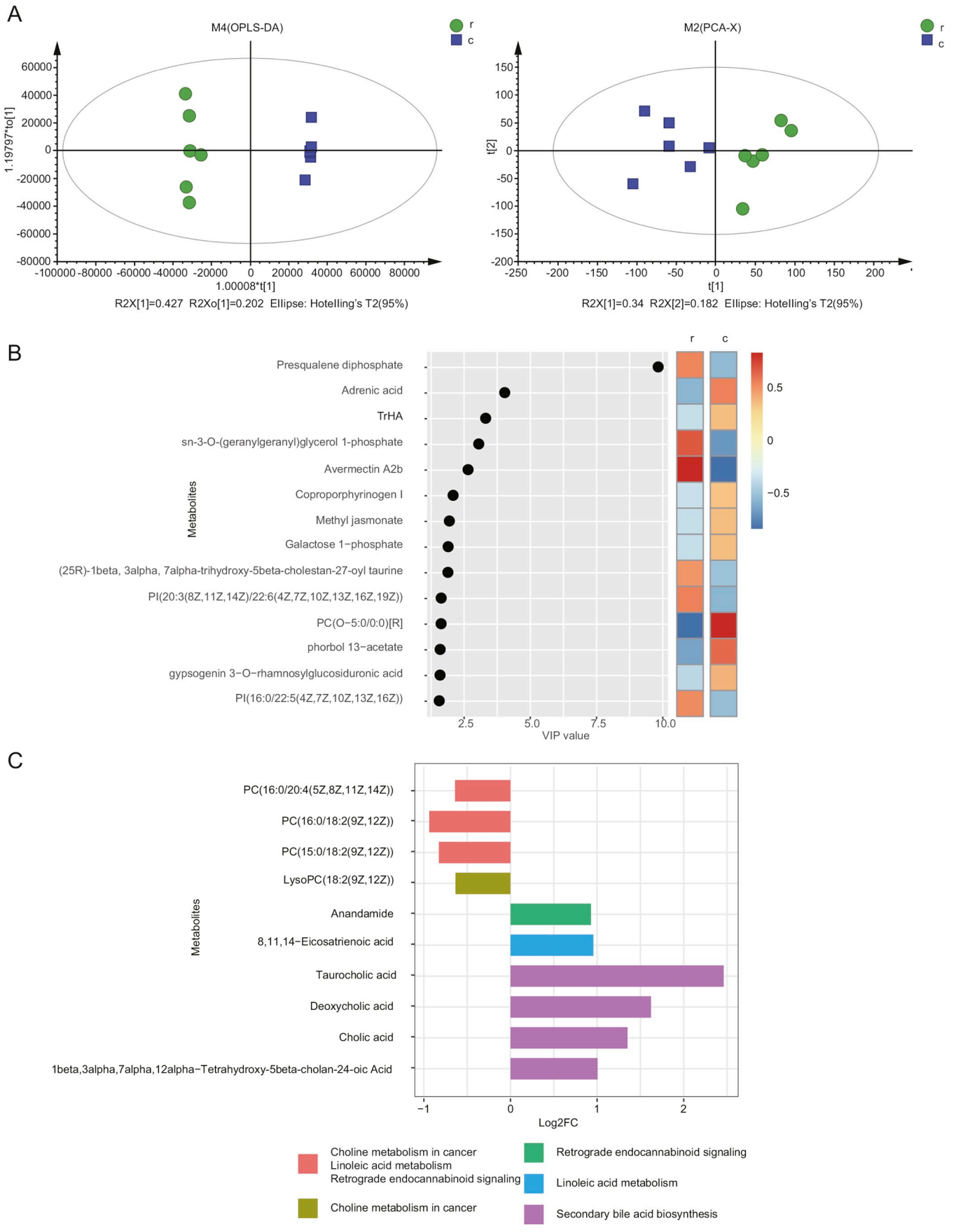

(caption on next page)

Fig. 4. liquid chromatography-mass spectrometry analysis (LC-MS)-based metabolomics analysis on enteric metabolome using fecal samples. (A): OPLS-DA and Principal Component Analysis (PCA) score scatter plots gotten from LC-MS data in M4 model and M2 model respectively. R2: the total explained variation of the model; shows the fitness of derived model for the data. Q2: the predictability of the model; reflects the model of quality. (B): Variable importance in projection (VIP) analysis based on OPLS-DA. (C): KEGG pathway enrichment of the significantly changed metabolites. Abbreviations: R: fecal samples from prion infected mice. C: fecal samples from healthy control mice.

3.3. Fecal metabolome analysis of the enteric changes in prion disease

To identify the specific enteric changes in prion disease, fecal metabolites from the infected and control groups (six samples randomly chosen from the two groups) were extracted and detected using an LC-MS–based metabolomics approach. As shown in Fig. 4A, the metabolite profiles of the infected and control groups were compared by OPLS-DA, which identifies the maximized difference between the two groups. This produced a two-component validated (cross-validated) model with a R^2Y of 0.996 and a Q^2 of 0.926. At the same time, PCA analysis (Fig. 4A) was performed to evaluate the profile differences between these two groups (R^2X = 0.522; Q^2 = 0.205). These two different analyses both indicated a good curve fit and satisfactory classification power. We used Student's *t*-test after OPLS-DA analysis for multiple testing. We identified 145 metabolites (VIP > 1.5, p < 0 .05) as having significant metabolic profiles, as is shown in Tables 1, 2 and Supplementary Table 1A. Of these 145 metabolites, 67 were decreased (FC < 1), and 78 metabolites were increased. Among those 78 increased metabolites, avermectin A2b (VIP = 2.60), sn-3-O-(geranylgeranyl)glycerol 1-phosphate (vip = 3.01), PI(20:3(8Z,11Z,14Z)/22:6(4Z,7Z,10Z,13Z,16Z,19Z)) (VIP = 1.59), presqualene diphosphate (VIP = 9.78), PI(16:0/22:5(4Z,7Z,10Z,13Z,16Z)) (VIP = 1.51), and (25*R*)-1beta,3alpha,7alpha-trihydroxy-5beta-cholestan-27-oyl taurine ((VIP = 1.84) displayed the most dramatic changes. PC(O-5:0/0:0)[R] (VIP = 1.58), phorbol 13-acetate, (VIP = 1.55), adrenic acid (VIP = 3.99), gypsogenin 3-O-rhamnosylglucosiduronic acid (VIP = 1.54), TrHA (VIP = 3.27), methyl jasmonate (VIP = 1.90), and galactose 1-phosphate (VIP = 1.85) displayed the most dramatic decreases, with FCs < 0.2. The VIP scores of these top metabolites were an indication of their contribution to the OPLS model (Fig. 4B). Among these 145 metabolites with significant metabolic profiles, only 13 of the 78 increased metabolites and 18 of the 67 decreased metabolites are not lipidic components (Supplementary Table 1B), indicating that prion infection may highly influence lipid or lipid-related metabolism.

To further identify pathways affected by prion disease, we performed KEGG pathway enrichment analysis on the 145 significant metabolites with known KEGG IDs (Fig. 4C). Ultimately, 10 metabolites were found to be significantly (VIP > 1.5, p < 0 .05) enriched in 4 pathways: choline metabolism in cancer, retrograde endocannabinoid signaling, linoleic acid metabolism, and secondary bile acid biosynthesis. Of these, only lysoPC(18:2(9Z,12Z)), which participates in choline metabolism, was decreased after prion disease, with a $\log_2$FC of −0.64. All 4 metabolites (taurocholic acid; 1beta, 3alpha, 7alpha,12alpha − tetrahydroxy − 5beta-cholan − 24 − oic acid; cholic acid; and deoxycholic acid) in secondary bile acid biosynthesis, 8,11,14 − eicosatrienoic acid in linoleic acid metabolism, and anandamide in retrograde endocannabinoid signaling were increased after prion disease. Strikingly, 3 metabolites (PC(16:0/20:4(5Z,8Z,11Z,14Z)), PC(16:0/18:2(9Z,12Z)), and PC(15:0/18:2(9Z,12Z))) involved in 3 of these metabolic pathways (choline metabolism in cancer, linoleic acid metabolism, and retrograde endocannabinoid signaling) were all decreased. These 3 decreased metabolites in distinct metabolic pathways were all PC-related compounds, which indicates that PC metabolism may be perturbed. The observation that host metabolites displayed significant changes in the prion-infected samples provides evidence that prion disease will cause significant shifts in host metabolism.

3.4. Changes in SCFA and amino acid concentrations in fecal samples

It has been gradually demonstrated that SCFAs and amino acids can modulate neural function and neuroimmune responses and are altered in many neural diseases. To further investigate the exact types and concentrations of SCFAs and amino acids in fecal samples from the infected and control groups, we randomly chose 5 samples from each group to extract and detect SCFAs using a GC–MS–based metabolomics approach as well as 3 samples from each group to extract and detect 20 proteinogenic amino acids using an ultra-performance liquid chromatography (UPLC) approach (Supplementary Table 2A, B). We detected 8 types of SCFAs (Fig. 5A, B), including acetic acid, propionic acid, isobutyric acid, butyric acid, isovaleric acid, valeric acid, isohexanoic acid, and caproic acid. Interestingly, we were unable to detect isovaleric acid in all 5 samples in each group, and the concentrations of these 8 types of SCFAs were all higher in the control group than in the infected group, as all eight fold change (FC) scores show significant difference. Acetic acid was the most abundant, followed by butyrate, and isohexanoic acid was the least abundant. Caproic acid displayed the most dramatic decrease of all SCFAs (FC = 6.85), and acetic acid changed the least (FC = 1.573). The decreases in acetate, butyric acid, and propionate resulted in FC scores of 1.57, 1.61, and 1.81, respectively. We also detected 20 amino acids (Fig. 5C, D) found in proteins (His, Asn, Ser, Gln, Arg, Gly, Asp, Glu, Thr, Ala, Pro, Cys, Lys, Tyr, Met, Val, Ile, Leu, Phe, and Trp) using the Waters ACCQ-Tag method. Four amino acids were not detected (Asp, Glu, Pro, and Lys), and 14 amino acids were found to decrease upon prion infection (His, Asn, Ser, Gln, Arg, Gly, Thr, Ala, Met, Val, Ile, Leu, Phe, and Trp). Additionally, His and Trp were not detected after prion disease infection, indicating that these two amino acids were dramatically decreased. Arg also decreased significantly, with an FC score of 0.627. In contrast, the concentrations of Cys and Tyr increased, with FC scores of 1.269 and 1.241, respectively. These data demonstrate that prion disease causes decreases of all types of SCFAs, and 14 amino acids markedly decreased while 2 increased.

3.5. Correlations between the fecal metabolome and gut microbiome

To investigate the correlations between the differential gut microbiota and the enteric changes described above, the Spearman correlation coefficient was computed for the 145 differential metabolites and 4 family-level bacterial taxa (the relative abundance was > 3%), as detected by both STAMP and LEfSe analyses (Fig. 6A). We uncovered 43 statistically significant interactions between 26 metabolites and 4 bacterial taxa (p < 0 .05). Remarkably, the increase in *Lactobacillaceae* after prion disease infection was shown to be correlated with 22 differential metabolites: 7 lipids and lipid-like molecules, 2 nucleosides and analogues, 4 organic acids, 3 organic oxygen compounds, 2 organic nitrogen compounds, 2 organoheterocyclic compounds, 1 organo-oxygen compound, and 1 polyketide. Pantothenic acid was found to have the strongest positive correlation with *Lactobacillaceae*, and xanthine, taurocholic acid, deoxycholic acid, taurodeoxycholic acid, and 19 − norandrosterone displayed strong positive correlations with *Lactobacillaceae* (r > 0.7, p < 0 .01). *Helicobacteraceae* also exhibited a significant increase in prion disease, but it was shown to be only weakly related to several metabolites. Two other bacterial families, *Prevotellaceae* and *Ruminococcaceae*, were shown to decrease in prion disease. There were 15 metabolites correlated with *Prevotellaceae*: 4 lipids and lipid-like molecules, 3 nucleosides and analogues, 3 organic acids, 4 organic oxygen compounds, and 1 organic nitrogen compound.

Table 1
Significant increased metabolites in prion infection groups when compared with healthy controls using OPLS-DA. Abbreviations: FC, fold-change. VIP value, The variable importance in projection.

Metabolites	Ion mode	FC (R/C)	VIP value	*p* Value
Avermectin A2b	POS	47.75663	2.60294	.021368
sn-3-O-(geranylgeranyl)glycerol 1-phosphate	NEG	23.22366	3.00541	.020079
PI(20:3(8Z,11Z,14Z)/22:6(4Z,7Z,10Z,13Z,16Z,19Z))	NEG	12.90806	1.58797	3.24E-06
Presqualene diphosphate	NEG	12.63776	9.7803	.002854
PI(16:0/22:5(4Z,7Z,10Z,13Z,16Z))	NEG	11.542	1.51378	2.48E-05
(25*R*)-1beta,3alpha,7alpha-trihydroxy-5beta-cholestan-27-oyl taurine	NEG	10.05392	1.84116	4.35E-07
SQDG(22:5(5Z,8Z,11Z,14Z,17Z)/16:1(13Z))	POS	9.121172	3.30602	.000369
Taurodeoxycholic acid	NEG	8.122847	3.57406	.000816
Leukotriene B4	NEG	6.654625	1.84084	.005762
Cucurbitacin F	NEG	6.238219	1.71572	.003418
6E,8E,12E,14E-Hexadecatetraen-10-ynoic acid	POS	5.681119	1.6491	.014548
Taurocholic acid	NEG	5.51123	8.77795	1.14E-05
PS(22:6(4Z,7Z,10Z,13Z,16Z,19Z)/20:4(5Z,8Z,11Z,14Z))	NEG	5.498881	5.4359	.000122
Adenine	POS	5.09072	3.33501	.007185
Brosimone H	NEG	4.880999	1.88048	.000352
PI(16:0/18:0)	POS	4.794187	3.0295	.010166
sarmentogenin	POS	4.711024	5.06516	.000269
Stoloniferone J	NEG	4.483258	1.96417	.002783
3alpha,12beta-Dihydroxy-11-oxo-5beta-cholan-24-oic Acid	POS	4.421034	2.90548	.000765
1alpha,23-dihydroxy-24,25,26,27-tetranorvitamin D3/1alpha,23-dihydroxy-24,25,26,27-tetranorcholecalciferol	NEG	4.269869	3.70787	1.67E-07
6-Bromo-5E,9Z,13Z,24Z-heptacosatetraenoic acid	NEG	3.73236	2.13067	1.39E-07
Neolinderatin	NEG	3.670285	2.29993	.0089
Estrone	POS	3.665394	1.55254	.007906
(+)-Blennin D	NEG	3.433452	1.52032	.000356
THA	POS	3.227018	5.19638	.000419
N-oleoyl asparagine	POS	3.220928	2.145	.002258
Nandrolone	POS	3.166351	1.5353	.000325
PI(17:2(9Z,12Z)/0:0)	POS	3.147376	1.60431	.001143
Deoxycholic acid	POS	3.079159	22.4291	7.3E-05
3beta-(3-methyl-butanoyloxy)-villanovane-13alpha,17-diol	NEG	3.068957	15.701	1.21E-05
Methylmalonic acid	POS	3.056	2.24833	.012324
3,7,11-Trimethyl-2,6,10-dodecatrienyl acetate	POS	2.83637	1.54912	.000333
4-[5]-ladderane-butanoic acid	POS	2.665319	1.96024	.000409
geodisterol-O-sulfite	NEG	2.650776	3.34805	.001598
Cytosine	POS	2.597388	2.5242	5.81E-05
30:6(12Z,15Z,18Z,21Z,24Z,27Z)	POS	2.562626	7.31443	.000906
Cholic acid	POS	2.552187	17.4507	5.63E-05
delta2-THA	POS	2.32388	18.3368	.000137
(+)-Myristinin A	POS	2.296649	2.64583	.000123
Oleanolic acid	POS	2.278991	2.20367	.009636
17beta-Estradiol 3-(beta-D-glucuronide)	POS	2.265179	2.034	.000348
Kazinol E	POS	2.254631	2.10322	.001275
3-O-(alpha-L-rhamnopyranosyl-(1–2)-alpha-L-rhamnopyranosyl)-3-hydroxydecanoic acid	POS	2.223808	1.87161	.000174
3alpha-Hydroxy-12-oxo-5beta-cholan-24-oic Acid	NEG	2.191753	4.97606	.023939
Taurine	NEG	2.176465	3.05086	.034061
PA(P-18:0/0:0)	NEG	2.146724	1.94797	.001016
2,6,8,12-Tetramethyl-2,4-tridecadien-1-ol	NEG	2.137912	4.40425	.008084
plastoquinol-1	POS	2.094619	2.64378	7.66E-05
L-Malic acid	POS	2.085828	2.03954	.001108
L-Methionine	NEG	2.076903	1.80841	.038994
4,8-Dimethyl-4E,8E-decadien-10-olide	POS	2.068962	2.22067	7.12E-05
13-Dihydrodaunorubicin	POS	2.06803	2.82755	.000262
N-Oleoylethanolamine	POS	2.067133	1.56776	.010979
VD 2716	POS	2.033754	2.57679	4.57E-05
2-deoxyecdysone 22-phosphate	POS	2.033024	2.92751	3.05E-06
1beta,3alpha,7alpha,12alpha-Tetrahydroxy-5beta-cholan-24-oic Acid	POS	2.008058	2.77056	.001066
Thymine	POS	1.971141	1.79463	.010089
10-Hydroxy-isolaurene	POS	1.968588	1.52774	.000134
8,11,14-Eicosatrienoic acid	POS	1.94238	1.94284	.004725
19-Norandrosterone	POS	1.941686	1.54864	2.58E-05
Anandamide	POS	1.904742	1.55553	.009057
20-hydroxyecdysone 22-phosphate	POS	1.855139	2.85491	3.19E-05
Cer(d18:2/18:1)	POS	1.854968	2.13758	.001648
PI(13:0/0:0)	POS	1.842183	1.7257	4.33E-05
Sophoradochromene	POS	1.809638	1.62367	.000726
24,25-epoxy-1alpha-hydroxyvitamin D3/24,25-epoxy-1alpha-hydroxycholecalciferol	POS	1.72995	1.7313	.002291
N-Acetylneuraminic acid	POS	1.695278	1.91351	.014294
3,4,7-Trihydroxy-5-methoxy-8-prenylflavan 7-O-beta-D-glucopyranoside	POS	1.68461	2.76293	.000134
Malvidin 3-glucoside-5-(6-acetylglucoside)	NEG	1.656785	1.83613	.000564
Scilliroside	POS	1.652389	1.51224	.01095
7-oxo-11E-Tetradecenoic acid	NEG	1.643487	2.54858	9.18E-05
Artoindonesianin A	NEG	1.608029	1.72475	.000716
Pantothenic acid	POS	1.582558	2.48344	.001893

(*continued on next page*)

Table 1 (*continued*)

Metabolites	Ion mode	FC (R/C)	VIP value	*p* Value
Iso-Valeraldehyde	POS	1.582419	2.45219	.040858
Dorsilurin E	POS	1.551183	1.99795	.001515
14-O-(beta-D-glucopyranosyl)-7S,14R-dihydroxy-7,9,13,17-tetramethyl-2E,4E,8E,10E,12E,16E-octadecahexaenoic acid	NEG	1.451649	1.62723	.013618
Xanthine	NEG	1.446129	2.64876	.008977
stigmast-5-en-3beta-ol 3–0-beta-D-glucopyranoside	NEG	1.172357	1.7563	.020793

Pseudouridine displayed the strongest positive correlation, and xanthosine, ribothymidine, D-glucuronic acid, and D-maltose also displayed strong positive correlations ($r > 0.7$, $p < 0.01$). L-Malic acid was the most negatively correlated among the 3 negative metabolites. Six metabolites were found to have negative interactions with *Ruminococcaceae*: deoxycholic acid, taurodeoxycholic acid, nandrolone, thymine, xanthine, and pantothenic acid, which displayed the most negative correlation ($|r| > 0.4$, $p < 0.05$).

To further investigate the relationship of the fecal metabolites with the gut microbial changes, we performed redundancy analysis (RDA) with 8 differential metabolites with VIP scores > 8 as 'environmental variables' and the relative abundance of OTUs (based on different bacteria at the family level) as 'species variables' (Fig. 6B). In total, the 8 tested metabolites contributed 74.23% of the changes to the bacterial OTUs. The infected and control groups displayed good separation into 2 groups, and individuals within each group showed a good internal correlation. Two metabolites, PC(16:0/18:2(9Z,12Z)) and 22S,23S-epoxy-5alpha-stigmast-8(9),14(15)-dien-3beta-ol, are related to *Ruminococcaceae* and *Prevotellaceae*, which are associated with the control group, while six metabolites (delta2-THA; deoxycholic acid; cholic acid; 3beta-(3-methyl-butanoyloxy)-villanovane-13alpha,17-diol; taurocholic acid; and presqualene diphosphate) are related to *Lactobacillaceae* and *Helicobacteraceae*, which are associated with the infected group. These 6 metabolites exhibit similar distances from each other, indicating that they are similar environmental variables for the observed variation in the gut microbiota in prion infection. Deoxycholic acid, which displayed the top VIP (22.43), is a type of secondary bile acid, which are metabolic byproducts of intestinal bacteria. This suggests that the observed alterations in fecal metabolites upon prion infection are likely derived from the gut microbiota. Taken together, the observed strong correlations between the gut microbial changes and shifted metabolic levels indicate that prion disease can result in significant changes in the gut microbiota, which result in dramatic shifts in host metabolites.

4. Discussion

In our study, we revealed that fecal samples from mice with prion disease had a fecal microbiome distinct from that of the healthy littermates. Results of 16S rRNA–based microbiome analysis indicated that the gut microbiota of the prion-infected group was significantly different. Using alpha diversity metrics (richness and diversity), we found that the gut microbiota of healthy samples were richer at the family and phylum levels, and individual members displayed higher stability. Using beta diversity, we qualitatively observed that the gut microbial structure of the infected group differed significantly from that of the healthy group. Taken together, these results indicate that the gut microbiota of the prion diseaseinfected individuals was imbalanced.

LEfSe analysis of bacterial taxa indicated that 2 bacterial phyla displayed significant differences in their abundance upon prion infection; *Proteobacteria* increased and *Saccharibacteria* decreased. These two bacterial phyla also contain three of the bacterial taxa that displayed differential levels, indicating that the main taxa-level changes occurred in these two phyla. As found in previous studies, *Proteobacteria* contain a wide range of disease-causing pathogens, including *Escherichia, Salmonella, Vibrio,* and *Helicobacter*. The increased prevalence of *Proteobacteria* is a signal of an unstable microbial community (dysbiosis) and a potential diagnostic criterion for disease (Na-Ri et al., 2015). Outgrowth of *Proteobacteria* has been found to induce an innate immune response and promote intestinal inflammation via immunoregulatory cytokines (Maharshak et al., 2013). Several studies have found that *Saccharibacteria* is one of the most abundant and widespread phyla in nature due to its diverse habitats, which include human and dolphin oral cavities, animal gastrointestinal tracts, soil, and activated sludge (Starr et al., 2018). While the physical functions of this phyla in the host remain obscure, recent studies have found that the metabolism of *Saccharibacteria* influences the immunosuppressive capabilities of an episymbiont of *Actinomyces odontolyticus* in human mouths and is related to several digestive diseases (Opdahl et al., 2018). Further investigation of the specific function of *Saccharibacteria* in the host may reveal the role of *Saccharibacteria* in prion disease infection. Interestingly, overrepresentation of *Proteobacteria*, combined with a low representation of *Saccharibacteria*, may be associated with depression (Tillmann et al., 2019). Given these findings, we suspect *Proteobacteria* and *Saccharibacteria* may be involved in intestinal and extraintestinal inflammation and other metabolic reactions, which cause mental and physical changes and intensify disease after prion disease infection, as prion disease infected sheep commonly display subtle temperament changes and nonspecific signs, such as listlessness. We observed significant increased species richness after infection; at the family level, altered members include *Lactobacillaceae* and *Helicobacteraceae*, while *Prevotellaceae* and *Ruminococcaceae* decreased. Interestingly, these observations are similar to those made for PD. Studies demonstrate a reduction of *Prevotellaceae* and an increase of *Lactobacillaceae* and *Helicobacteraceae* in fecal samples of PD patients. Further investigations found that the decreased level of *Prevotellaceae* in PD may be related to increased gut permeability intensifying the translocation of bacterial antigens (Forsyth et al., 2011). Moreover, the increased prevalence of *Helicobacteraceae*, known as the pathogenic bacterium associated with gastrointestinal diseases (Castiglioni et al., 2012; Sallas et al., 2019) may further cause motor impairments and gastrointestinal tract damage in PD (Çamcı and Oğuz, 2016). Considering these previous discoveries, we suspect that these 4 family-level bacterial taxa may play similar roles in the host after prion infection, which requires further investigation. ROC curve analysis also confirmed the correlation between these different bacterial taxa and prion infection, which is powerful evidence demonstrating this functional relationship.

In our study, we demonstrated a striking metabolic shift in the gut environment in prion disease. We detected a total of 145 significant metabolites, 78 of which increased and 67 of which decreased (using FC and VIP scores). Among the top 6 dramatically increased metabolites, avermectin A2b belongs to avermectins used as pesticides to treat parasites and insects, which have been found to have toxic effects on the nervous and metabolic systems of non-target organisms (Cully et al., 1994; Sun et al., 2010). In AD avermectins have not only been identified as modifiers of amyloid precursor protein, but also increase short amyloid β peptides at the expense of longer and potentially more toxic forms (Brownjohn et al., 2017). Some reports, including our previous studies, found that avermectin could impair mitochondrial bioenergetics, induce oxidative stress, and modify cell structures, and influence immune function (Li et al., 2018; Zanoli et al., 2012), which could further intensify PrP^{Sc} aggregation and neuronal death. Especially in

Table 2
Significant decreased metabolites in prion infection groups when compared with healthy controls using OPLS-DA. Abbreviations: FC, fold-change. VIP value, variable importance in projection.

Metabolites	Ion mode	FC (R/C)	VIP value	*p* Value
PC(O-5:0/0:0)[R]	POS	0.022599	1.58429	.000227
phorbol 13-acetate	NEG	0.056099	1.54842	5.59E-05
Adrenic acid	NEG	0.076099	3.98692	.009641
gypsogenin 3-O-rhamnosylglucosiduronic acid	POS	0.156555	1.54409	.002987
TrHA	POS	0.183877	3.26712	.009356
Methyl jasmonate	NEG	0.188977	1.89603	9.69E-07
Galactose 1-phosphate	POS	0.195139	1.85036	2.47E-05
Coproporphyrinogen I	NEG	0.203967	2.03775	.002879
14-hydroxy-12-tetradecenoic acid	NEG	0.20962	2.71122	.00062
2-deoxy-20-hydroxyecdysone 22-phosphate	NEG	0.226038	1.72952	.003286
Xanthosine	NEG	0.227869	2.16315	.000335
1alpha,25-dihydroxy-26,27-dimethyl-20,21-methano-23-oxavitamin D3/1alpha,25-dihydroxy-26,27-dimethyl-20,21-methano-23-oxacholecalciferol	POS	0.266664	1.57684	.003073
Derricin	POS	0.267778	1.63743	.000106
Epsilon-(gamma-Glutamyl)-lysine	POS	0.283339	1.78265	6.08E-07
5,7,4′-Trihydroxy-3″-methoxy-6,8-di-*C*-methylflavanone	NEG	0.298203	2.72201	.000713
Heptadecanoic acid	POS	0.29914	1.85663	.01638
22S,23S-epoxy-5alpha-stigmast-8(9),14(15)-dien-3beta-ol	POS	0.304345	8.28314	.006176
Riboflavin	NEG	0.315902	1.72323	.005518
N-heptanoyl-homoserine lactone	POS	0.317425	4.50971	.000129
Pinnasterol	NEG	0.32226	3.98801	.011165
26,26,26,27,27,27-hexafluoro-25-hydroxyvitamin D2	POS	0.326912	2.61441	5.96E-06
Phytanic acid	POS	0.344637	2.01651	.020478
PG(18:0/0:0)	NEG	0.350075	3.43659	.014103
Metanephrine	POS	0.37143	3.1247	5.1E-06
PA(20:1(11Z)/0:0)	NEG	0.383562	4.64133	.003242
Ecgonine methyl ester	POS	0.387779	2.92642	8.07E-05
Peridinin	POS	0.396301	2.07913	.001
Norselic acid E	POS	0.407789	1.82081	.009384
Sophoracoumestan A	NEG	0.413373	2.52914	.000936
PG(P-18:0/0:0)	POS	0.413842	1.75904	.003932
PA(18:0/0:0)	NEG	0.423507	4.2777	.007846
Methylimidazoleacetic acid	POS	0.430498	2.54744	.015228
PS(18:0/0:0)	NEG	0.444428	2.20165	.009727
PG(P-16:0/0:0)	POS	0.467144	1.92224	.00633
Pseudouridine	NEG	0.467916	1.89566	.002749
Isomaltose	NEG	0.474936	1.61241	.004869
PS(18:4(6Z,9Z,12Z,15Z)/0:0)	POS	0.476213	1.84057	.001327
Ustilagic acid	POS	0.48674	1.9822	.014696
Tanariflavanone A	POS	0.488255	2.58152	.000422
Norselic acid B	NEG	0.491091	3.59077	.003914
PE(P-18:1(11Z)/22:6(4Z,7Z,10Z,13Z,16Z,19Z))	POS	0.50851	1.72096	.029411
PG(16:0/0:0)	POS	0.516075	1.90479	.009035
PC(16:0/18:2(9Z,12Z))	POS	0.521821	9.99032	.049901
Porphobilinogen	POS	0.536259	1.57217	.000195
Ribothymidine	POS	0.562792	1.58297	3.11E-06
PC(15:0/18:2(9Z,12Z))	POS	0.563568	1.68529	.041467
4alpha-carboxy-4beta-methyl-zymosterol	POS	0.570832	2.69368	.035235
PA(O-20:0/20:3(8Z,11Z,14Z))	POS	0.582317	2.362	.000363
27:2(5Z,9Z)(6Br)	POS	0.593949	2.46331	.000969
1-(O-alpha-D-glucopyranosyl)-29-keto-(1,3*R*,31*R*)-dotriacontanetriol	POS	0.594553	2.50934	.005575
Cucurbitacin E	NEG	0.597734	1.82241	.02917
MG(16:0/0:0/0:0)[rac]	POS	0.619029	2.0173	.001983
D-Maltose	POS	0.632608	1.74422	.001529
PE(22:6(4Z,7Z,10Z,13Z,16Z,19Z)/0:0)	POS	0.633684	2.56135	.005026
N-(6-aminohexanoyl)-6-aminohexanoic acid	POS	0.63766	1.6102	.000333
PC(16:0/20:4(5Z,8Z,11Z,14Z))	POS	0.641458	4.12674	.001207
LysoPC(18:2(9Z,12Z))	POS	0.643749	1.75175	.026313
L-Tyrosine	NEG	0.652968	2.7227	4.89E-05
Glycylproline	POS	0.658287	2.35218	3.63E-05
DHA (d5)	POS	0.684849	1.78079	.024414
PC(4:0/4:0)	POS	0.687738	1.69332	.000374
D-Glucuronic acid	NEG	0.700275	1.66375	.015897
Pipecolic acid	POS	0.735253	1.7732	.009202
EPA (d5)	POS	0.797532	2.15838	.001333
PA(O-16:0/22:4(7Z,10Z,13Z,16Z))	POS	0.797873	1.73461	3.32E-05
PA(16:0/22:6(4Z,7Z,10Z,13Z,16Z,19Z))	POS	0.820122	1.59039	.00559
TG(14:0/14:0/19:1(9Z))[iso3]	POS	0.856111	1.51091	.000636

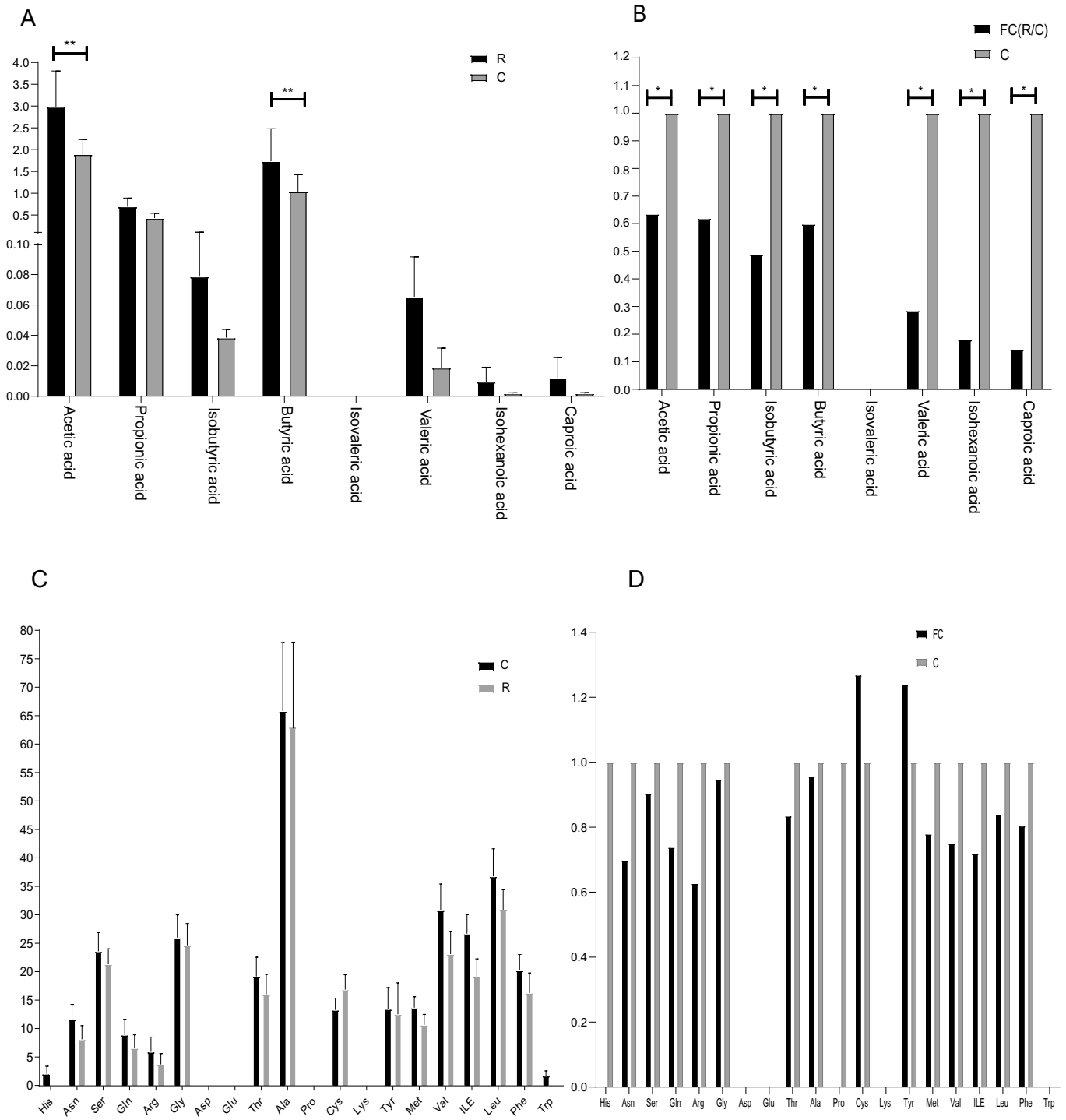

Fig. 5. Detection of absolute concentration of SCFAs and amino acids in prion infectious groups and healthy control groups. (A): The absolute concentration of 8 types of SCFAs in prion infectious groups and healthy controls. (B): The FC score histogram of 8 types of SCFAs in prion infectious groups and healthy controls. $*p < 0.05$, $**p < 0.01$. (C): The absolute concentration of 20 proteinogenic amino acids in prion infectious groups and healthy controls. (D): The FC score histogram of 20 proteinogenic amino acids in prion infectious groups and healthy controls. Data was expressed as mean ± SEM. Difference of data subjects were assessed using the *t*-test, $*p < 0.05$, $**p < 0.01$. Abbreviations: R: fecal samples from prion infected mice. C: fecal samples from healthy control mice.

the early stages of prion disease, reduced exercise tolerance and weight loss are commonly seen. The metabolites sn-3-O-(geranylgeranyl)glycerol 1-phosphate, PI(20:3(8Z,11Z,14Z)/22:6(4Z,7Z,10Z,13Z,16Z,19Z)), and PI(16:0/22:5(4Z,7Z,10Z,13Z,16Z)) are all in glycerophospholipids (PI), which are widely distributed in the body and function in forming biological membranes and signaling molecules. Although little is known about the role of PI in neural diseases, increased PI was observed in schizophrenia, depression, and the lipid rafts of the frontal cortex from PD patients (Farooqui et al., 2000; Hibbeln and Salem Jr., 1995). Meanwhile, most of the significantly decreased metabolites in prion infection are lipid or lipid-like compounds, indicating a significant change in lipid metabolism. Through a correlation analysis of the microbiome and metabolome as well as an RDA analysis, deoxycholic acid, cholic acid, and taurocholic acid were

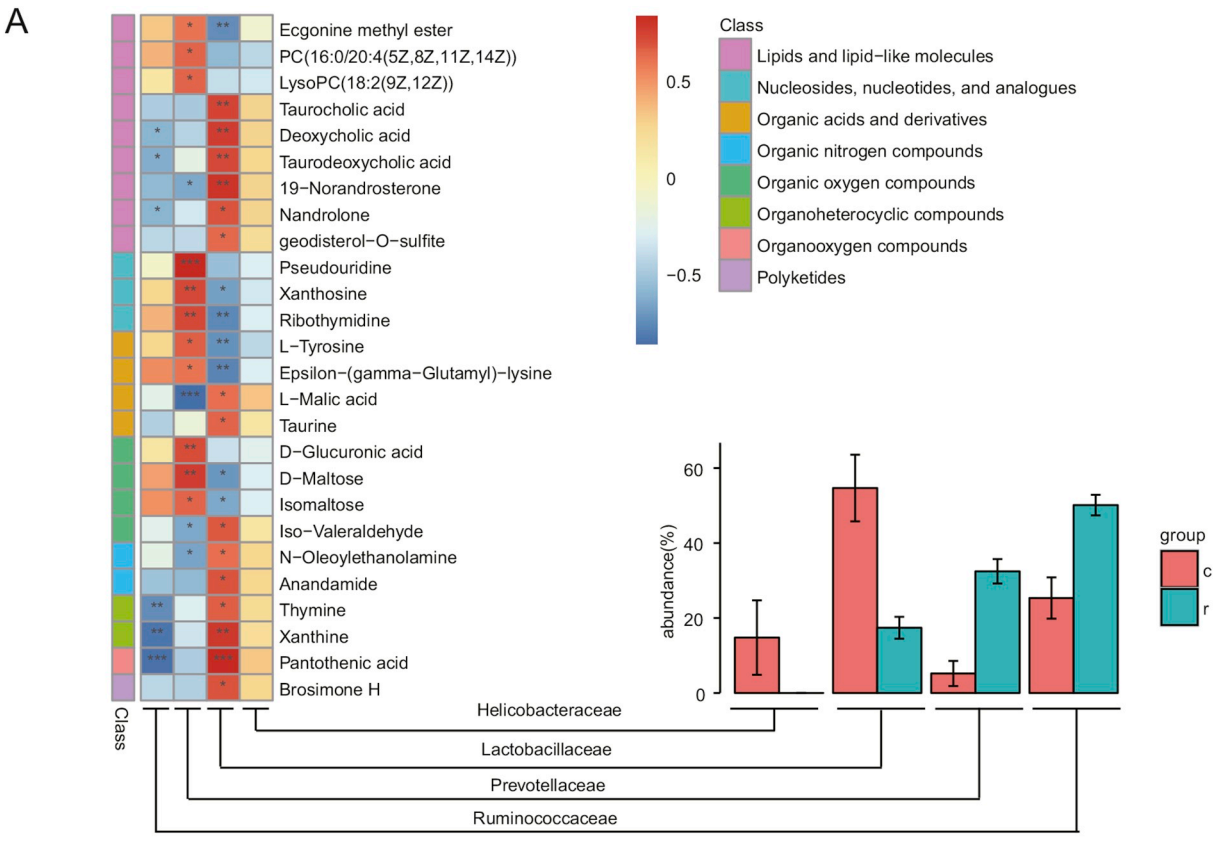

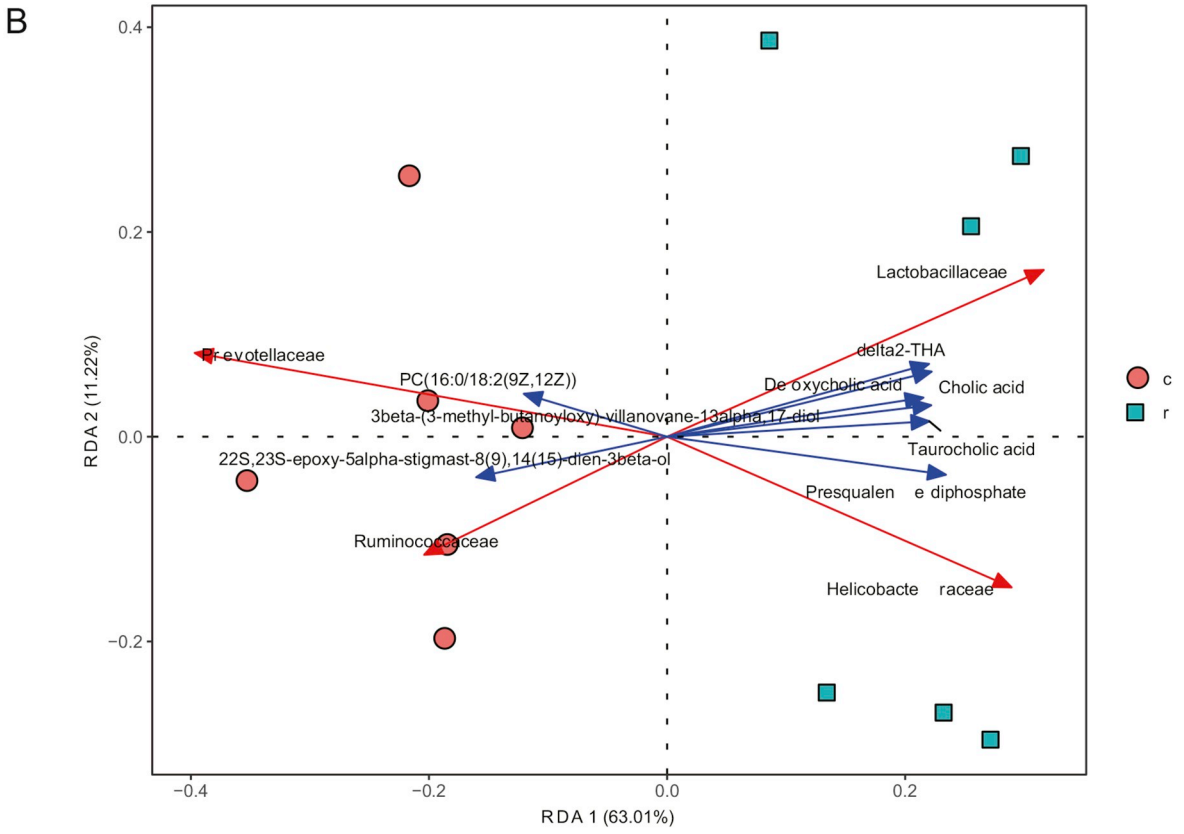

(caption on next page)

Fig. 6. Correlation between the fecal metabolome and gut microbiota. (A): Correlation analysis of fecal metabolome and gut microbiota upon prion infection. Spearman correlation coefficient is computed for the relative abundant concentration of differential metabolites. Differentially abundant taxa of gut microbiota are selected by both STAMP and LEfSe analyses. (*$p < 0.05$,**$p < 0.01$,***$p < 0.001$). (B): Redundancy analysis (RDA) plot of fecal metabolome relative to gut microbiota. Responding gut microbiota are indicated by red arrows, Responding fecal metabolome are indicated by blue arrows. First and second plotted ordination axes together explain 63.01% and 11.22% of the proportion of variance, respectively. Abbreviations: R: fecal samples from prion infected mice. C: fecal samples from healthy control mice. (For interpretation of the references to colour in this figure legend, the reader is referred to the web version of this article.)

identified as significant increases in prion infection (high VIP and FC scores). These are all involved in secondary bile acid biosynthesis showing in the KEGG enrichment analysis of significantly changed metabolites, which indicates secondary bile acid biosynthesis were significantly affected. Moreover, increased hydrophobic bile acids indicates injury to the liver and disruption of the energy cycle (González-Flecha et al., 1993), and disorder of liver function may be related to depression (Burnham et al., 2014). These findings align with the clinical symptoms of prion disease infection, which include anorexia, lethargy, and in the later stage, emaciation. These hydrophobic bile acids may act as inflammatory agents that cause injury to the liver, intestine, and rest of the digestive system during prion infection. Remarkably, 3 metabolites [PC(16:0/20:4(5Z,8Z,11Z,14Z)), PC(16:0/18:2(9Z,12Z)), PC(15:0/18:2(9Z,12Z))] involved in 3 different metabolic pathways, but also related to phosphatidylcholine (PC), display a clear decrease during prion infection. PCs are essential components of cell membranes and comprise the majority of the total choline compound pool in most tissues (Frisardi et al., 2011). PCs are involved in anti-inflammation mechanisms, cholesterol metabolism, neuronal differentiation, and mitochondrial function (Marcucci et al., 2010; Schuler et al., 2015). Moreover, PCs are a precursor for sphingolipids that participate in the formation of the lipid rafts where GPI proteins are anchored. Sphingolipid depletion in neuroblastoma cells causes increased formation of PrP^{Sc} in prion infection (Naslavsky et al., 1999). Additionally, PCs are produced by a complex mechanism that involves the endoplasmic reticulum and mitochondria indicated (Friedman et al., 2018) that changes in PCs may reflect dysfunctions between these two organelles (Area-Gomez et al., 2018). Likewise, a recent study that analyzed large AD metabolomics datasets found dysregulation of inflammation and lipid metabolism, especially of sphingomyelins and ether-containing phosphatidylcholines, in preclinical biomarker-defined AD stages (Toledo et al., 2017). Meanwhile we find that phosphatidylethanolamine (PE), phosphatidylserine (PS) also display significant decreases among our 145 significantly shifted metabolites. Thus, we suspect that lipid metabolism especially bile acid and PC metabolism may be significantly altered in prion disease, and related metabolites in these pathways may further cause several clinical symptoms.

SCFAs and common amino acids are essential for host health-promoting neuroactive functions, especially inflammatory phenotypes (mediation of microglia) and neurotransmitter function in the neural system (Carroll et al., 2018; Erny et al., 2015). We detected SCFAs by GC–MS and common amino acids by UPLC. Remarkably, all SCFAs were markedly decreased, including acetate, propionate, and butyric acid. Previous studies discovered that SCFAs are able to connect to the gut-brain axis to regulate neural function (Devadder et al., 2014). Moreover, SCFAs (mainly of acetate, butyrate, and propionate) were found to be significantly decreased in PD patients (Unger et al., 2016) due to the under-representation of *Prevotellaceae*. Accordingly, we suspect that the decreases in *Prevotellaceae* may trigger decreases in SCFAs and further trigger intestinal damage and several immune cascade reactions in the gut. In our study, the levels of the amino acids Cys and Tyr increased, while His, Trp, and Arg decreased. The levels of Trp and His were below the limit of detection in the infected group. Notably, His exerts dramatic effects on immune complex clearance and phagocytosis of apoptotic cells. Decreases in His are expected to impair the immune response, which is initiated by histidine decarboxylase to produce histamine, and to intensify cognitive dysfunction, which may cause severe neuronal disorders (Jones et al., 2005; Song et al., 2018). Similarly, Trp-related metabolites, such as kynurenine, are widely involved in neuronal functions (Chiarugi et al., 2001). Tryptophan deficiency impaired the immune response and phagocytosis by macrophages. The observed low levels of His and Trp indicate a decreased level of immunity and disruption of the immune response and the nervous system that are further triggered after infection. At the same time, cysteine is the precursor of glutathione, which scavenges free radicals and other reactive oxygen species like hydroxyl radicals, lipid peroxyl radicals, and peroxynitrite (Dröge, 2005). The observed high level of Cys may be attributed to increased oxidative radicals, which may originate from significant changes in lipid metabolism. Additionally, in the brain, Thr and Gly can be converted into creatine, which can in turn provide phosphate groups for ADP to produce ATP (Tan et al., 2007). The observed decline of Thr and Gly suggests an energy deficiency after prion disease infection. Taken together, our findings demonstrate that SCFA and amino acid metabolism are clearly dysregulated in prion disease.

5. Conclusion

This study provides the first insight into the health impacts of prion disease infection from the perspective of the gut microbiota and host metabolism. Our data indicate that prion infection can result in significant gut microbial dysbiosis. Changes in certain bacterial taxa can further lead to striking metabolic changes in the host intestinal environment, as reflected in altered fecal metabolites. These findings highlight the specific disorder of the gut microbiota and striking metabolic changes that occur following prion infection. Integrated analysis of microbiome structure and fecal metabolites revealed important roles for four bacterial families in regulating the gut environment as well as significant changes in metabolites (avermectin A2b and glycerophospholipids). We observed the most changes in lipid metabolism pathways, including bile acid biosynthesis and choline-related metabolism, possibly due to prion infection. Therefore, our future research will focus on these four bacterial families and the metabolic changes caused by gut microbial dysbiosis as indicators of prion infection.

Supplementary data to this article can be found online at https://doi.org/10.1016/j.nbd.2019.104704.

Auther's contributions

YLF and ZDM designed and supervised the study. WW and YDM obtained the samples and clinical details. YDM performed 16S rRNA sequencing of the microbiota. YDM, YLF and WW performed the data analysis. SZAS assisted in statistical analysis of the metadata. YDM performed the metabolomic analysis. YDM wrote the manuscript. All authors read and approved the final manuscript.

Acknowledgements and funding sources

The authors thank Hongli Gao, Huafen Zhao, and Wen Li for their assistance in technical assistance. This work was supported by the Natural Science Foundation of China (Project No.31972641), National Key Research and Development Program (Project No. 2017YFC1200500, No.2017YFD0501600), 948 projects (2014-S9).

Declaration of competing interest

All of the authors have read and approved this manuscript, and due

care has been taken to ensure the integrity of the work. No part of this paper has been published or submitted elsewhere. The authors declare no conflicts of interest for the work described in this manuscript.

References

Abbott, R.D., et al., 2001. Frequency of bowel movements and the future risk of Parkinson's disease. Neurology 57, 456–462.

Area-Gomez, E., et al., 2018. A key role for MAM in mediating mitochondrial dysfunction in Alzheimer disease. Cell Death Dis. 9, 335.

Brownjohn, P.W., et al., 2017. Phenotypic screening identifies modulators of amyloid precursor protein processing in human stem cell models of Alzheimer's disease. Stem Cell Reports 8, 870.

Bruce, M.E., et al., 1997. Transmissions to mice indicate that 'new variant' CJD is caused by the BSE agent. Nature 389, 498–501.

Burnham, B., et al., 2014. Knowledge, attitudes, and beliefs of patients with chronic liver disease. Am. J. Health Behav. 38 (5), 737–744.

Çamcı, G., Oğuz, S., 2016. Association between Parkinson's disease and *Helicobacter pylori*. J. Clin. Neurol. 12, 147.

Carroll, J.A., et al., 2018. Microglia are critical in host defense against prion disease. J. Virol. 92 (15), e00549-18.

Castiglioni, V., et al., 2012. *Enterohepatic helicobacter* spp. in colonic biopsies of dogs: molecular, histopathological and immunohistochemical investigations. Vet. Microbiol. 159, 107–114.

Chiarugi, A., Meli, E., Moroni, F., 2001. Similarities and differences in the neuronal death processes activated by 3OH-kynurenine and quinolinic acid. J. Neurochem. 77, 1310–1318.

Cully, D.F., et al., 1994. Cloning of an avermectin-sensitive glutamate-gated chloride channel from *Caenorhabditis elegans*. Nature 371, 707–711.

De Almeida, C.G., et al., 2005. The cellular prion protein modulates phagocytosis and inflammatory response. J. Leukoc. Biol. 77, 238–246.

Devadder, F., et al., 2014. Microbiota-generated metabolites promote metabolic benefits via gut-brain neural circuits. Cell 156, 84–96.

Donaldson, D.S., et al., 2016. Increased abundance of M cells in the gut epithelium dramatically enhances oral prion disease susceptibility. PLoS Pathog. 12, e1006075.

Dröge, W., 2005. Oxidative stress and ageing: is ageing a cysteine deficiency syndrome? Philos. Trans. Biol. Sci. 360, 2355–2372.

Erny, D., et al., 2015. Host microbiota constantly control maturation and function of microglia in the CNS. Nat. Neurosci. 18, 965.

Farooqui, A.A., Horrocks, L.A., Farooqui, T., 2000. Glycerophospholipids in brain: their metabolism, incorporation into membranes, functions, and involvement in neurological disorders. Chem. Phys. Lipids 106, 1–29.

Forsyth, C.B., et al., 2011. Increased intestinal permeability correlates with sigmoid mucosa alpha-Synuclein staining and endotoxin exposure markers in early Parkinson's disease. PLoS One 6, e28032.

Friedman, J.R., et al., 2018. Lipid homeostasis is maintained by dual targeting of the mitochondrial PE biosynthesis enzyme to the ER. Dev. Cell 44 261–270.e6.

Frisardi, V., et al., 2011. Glycerophospholipids and glycerophospholipid-derived lipid mediators: a complex meshwork in Alzheimer's disease pathology. Prog. Lipid Res. 50, 313–330.

Girolamo, F., Coppola, C.C., Ribatti, D., 2017. Immunoregulatory effect of mast cells influenced by microbes in neurodegenerative diseases. Brain Behav. Immun. 65, 68.

González-Flecha, B., Cutrin, J.C., Boveris, A., 1993. Time course and mechanism of oxidative stress and tissue damage in rat liver subjected to in vivo ischemia-reperfusion. J. Clin. Investig. 91, 456–464.

Heppner, F.L., et al., 2001. Transepithelial prion transport by M cells. Nat. Med. 7, 976.

Hibbeln, J.R., Salem Jr., N., 1995. Dietary polyunsaturated fatty acids and depression: when cholesterol does not satisfy. Am. J. Clin. Nutr. 62, 1–9.

Hilton, D.A., et al., 1998. Prion immunoreactivity in appendix before clinical onset of variant Creutzfeldt-Jakob disease. Lancet 352, 703.

Jones, A.L., Hulett, M.D., Parish, C.R., 2005. Histidine-rich glycoprotein: a novel adaptor protein in plasma that modulates the immune, vascular and coagulation systems. Immunol. Cell Biol. 83, 106.

Langille, M.G., et al., 2013. Predictive functional profiling of microbial communities using 16S rRNA marker gene sequences. Nat. Biotechnol. 31, 814.

Laura, M.C., et al., 2011. Follicular dendritic cell-specific prion protein (PrP) expression alone is sufficient to sustain prion infection in the spleen. PLoS Pathog. 7, e1002402.

Legname, G., et al., 2004. Synthetic mammalian prions. Science 305, 673.

Lei, E., Vacy, K., Boon, W.C., 2016. Fatty acids and their therapeutic potential in neurological disorders. Neurochem. Int. 95, 75–84.

Li, C., et al., 2018. DLP1-dependent mitochondrial fragmentation and redistribution mediate prion-associated mitochondrial dysfunction and neuronal death. Aging Cell 17.

Mabbott, N.A., et al., 2003. Follicular dendritic cell dedifferentiation by treatment with an inhibitor of the lymphotoxin pathway dramatically reduces scrapie susceptibility. J. Virol. 77, 6845–6854.

Maharshak, N., et al., 2013. Altered enteric microbiota ecology in interleukin 10-deficient mice during development and progression of intestinal inflammation. Gut Microbes 4, 316–324.

Manson, J.C., et al., 1994. 129/Ola mice carrying a null mutation in PrP that abolishes mRNA production are developmentally normal. Mol. Neurobiol. 8, 121–127.

Marcucci, H., et al., 2010. Phosphatidylcholine biosynthesis during neuronal differentiation and its role in cell fate determination. J. Biol. Chem. 285, 25382–25393.

Marshall, A., et al., 2018. Oral prion neuroinvasion occurs independently of PrPC expression in the gut epithelium. J. Virol. 92, e01010–e01018.

Montrasio, F., et al., 2000. Impaired prion replication in spleens of mice lacking functional follicular dendritic cells. Science 288, 1257–1259.

Na-Ri, S., Tae Woong, W., Jin-Woo, B., 2015. Proteobacteria: microbial signature of dysbiosis in gut microbiota. Trends Biotechnol. 33, 496–503.

Naslavsky, N., et al., 1999. Sphingolipid depletion increases formation of the scrapie prion protein in neuroblastoma cells infected with prions. J. Biol. Chem. 274, 20763–20771.

Opdahl, L.J., Gonda, M.G., St-Pierre, B., 2018. Identification of uncultured bacterial species from Firmicutes, Bacteroidetes and CANDIDATUS Saccharibacteria as candidate cellulose utilizers from the rumen of beef cows. Microorganisms 6, 17.

Prinz, M., Priller, J., 2014. Microglia and brain macrophages in the molecular age: from origin to neuropsychiatric disease. Nat. Rev. Neurosci. 15, 300–312.

Pryde, S.E., et al., 2002. The microbiology of butyrate formation in the human colon. FEMS Microbiol. Lett. 217, 133–139.

Rhee, S.H., Pothoulakis, C., Mayer, E.A., 2009. Principles and clinical implications of the brain-gut-enteric microbiota axis. Nat. Rev. Gastroenterol. Hepatol. 6, 306–314.

Sallas, M.L., et al., 2019. Status (on/off) of oipA gene: their associations with gastritis and gastric cancer and geographic origins. Arch. Microbiol. 201, 93–97.

Schuler, M.H., et al., 2015. Phosphatidylcholine affects the role of the sorting and assembly machinery in the biogenesis of mitochondrial beta-barrel proteins. J. Biol. Chem. 290 (44), 26523–26532.

Song, J., et al., 2018. Histidine alleviates impairments induced by chronic cerebral hypoperfusion in mice. Front. Physiol. 9, 662.

Starr, E.P., et al., 2018. Stable isotope informed genome-resolved metagenomics reveals that Saccharibacteria utilize microbially-processed plant-derived carbon. Microbiome 6, 122.

Sun, Y.J., et al., 2010. Effects of avermectins on neurite outgrowth in differentiating mouse neuroblastoma N2a cells. Toxicol. Lett. 192, 206–211.

Tan, B., Xie, M., Yin, Y., 2007. Amino acids and immune functions. Br. J. Nutr. 98, 237–252.

Tillmann, S., et al., 2019. Altered fecal microbiota composition in the Flinders sensitive line rat model of depression. Psychopharmacology 236 (5), 1445–1457.

Toledo, J.B., et al., 2017. Metabolic network failures in Alzheimer's disease-A biochemical road map. Alzheimers Dement. 13, 965.

Unger, M.M., et al., 2016. Short chain fatty acids and gut microbiota differ between patients with Parkinson's disease and age-matched controls. Parkinsonism Relat. Disord. 32, 66–72.

Zanoli, J.C.C., et al., 2012. Abamectin affects the bioenergetics of liver mitochondria: a potential mechanism of hepatotoxicity. Toxicol. in Vitro 26, 51–56.